ARTIFICIAL SATELLITES, Vol. 55, No. 2 - 2020
DOI: 10.2478/arsa-2020-0004

PERFORMANCE ANALYSIS OF STATIC PRECISE POINT POSITIONING USING OPEN-SOURCE GAMP

Jabir Shabbir Malik
Phd scholar, School of Aerospace Engineering
Beijing Institute of Technology, 100081 Beijing, CHINA

ABSTRACT: In addition to Global Positioning System (GPS) constellation, the number of Global Navigation Satellite System (GLONASS) satellites is increasing; it is now possible to evaluate and analyze the position accuracy with both the GPS and GLONASS constellation. In this article, statistical analysis of static precise point positioning (PPP) using GPS-only, GLONASS-only, and combined GPS/GLONASS modes is evaluated. Observational data of 10 whole days from 10 International GNSS Service (IGS) stations are used for analysis. Position accuracy in east, north, up components, and carrier phase/code residuals is analyzed. Multi-GNSS PPP open-source package is used for the PPP performance analysis. The analysis also provides the GNSS researchers the understanding of the observational data processing algorithm. Calculation statistics reveal that standard deviation (STD) of horizontal component is 3.83, 13.80, and 3.33 cm for GPS-only, GLONASS-only, and combined GPS/GLONASS PPP solutions, respectively. Combined GPS/GLONASS PPP achieves better positioning accuracy in horizontal and three-dimensional (3D) accuracy compared with GPS-only and GLONASS-only PPP solutions. The results of the calculation show that combined GPS/GLONASS PPP improves, on an average, horizontal accuracy by 12.11% and 60.33% and 3D positioning accuracy by 10.39% and 66.78% compared with GPS-only and GLONASS-only solutions, respectively. In addition, the results also demonstrate that GPS-only solutions show an improvement of 54.23% and 62.54% compared with GLONASS-only PPP mode in horizontal and 3D components, respectively. Moreover, residuals of GLONASS ionosphere-free code observations are larger than the GPS code residuals. However, phase residuals of GPS and GLONASS phase observations are of the same magnitude.

Keywords: International GNSS Service (IGS); Precise Point Positioning (PPP); Open Software Package;

1. INTRODUCTION

Precise point positioning (PPP) is a most popular positioning technique among GNSS community because of its high accuracy and flexibility. PPP uses precise satellite orbit and clock products generated by the International GNSS Service (IGS) (Kouba and Héroux, 2001). GNSS data have been extensively used for several applications such as positioning, navigation, and timing (PNT); geodesy and geodynamics; and Earth's atmosphere and surface tomographic studies (Dong and Jin, 2018). PPP requires significant time to ensure better

positioning accuracy to converge decimeter to centimeter (Cai and Gao, 2013). Multi-constellation GNSS PPP, that is, GPS, GLONASS, Galileo, and BeiDou integrated positioning, has the potential to significantly improve the positioning accuracy because of the increased number of visible satellites and the improved satellite sky distribution. The reliability of position solutions can be enhanced because of the higher measurement redundancy.

Several PPP models and software packages have been developed by different research and academic organizations. All PPP software and tools are based on fundamental measurement and algorithms. GNSS data analysis capabilities, PPP performance, and reliability can be investigated. Bernese is a commercial software developed at the Astronomical Institute of the University of Bern (AIUB) (Dach et al., 2009). Bernese software handles single-frequency (SF) and dual-frequency (DF) GPS and GLONASS observations. GIPSY/OASIS (GOA II) was designed and developed by the National Aeronautical and Astronautical Jet Propulsion Laboratory (NASA, JPL) (https://gipsy-oasis.jpl.nasa.gov/gipsy/index.php), which can process dual-frequency GPS observations. It provides station coordinates, clock offsets, and estimates of atmospheric products. The "GPS Toolkit" (GPSTk) is an open-source project developed by the Applied Research Laboratories of the University of Texas (ARL, UT) (Salazar et al., 2010). GPSTk consists of core library, mathematical functions, and source codes for GNSS community. GAMIT/GLOBK was developed by the Massachusetts Institute of technology (MIT), which is a comprehensive analysis package for GPS observations. The output of GAMIT contains 3D relative positioning and earth-rotation parameters (Herring et al., 2015). GNSS-Lab (gLAB), developed by Astronomy and Research Group at the Universitat Politecnica de Catalunya (UPC), is a multipurpose programming tool suit to process SF and DF of GPS and GLONASS measurements (Hernandez et al., 2010). RTKLIB is an open-source software for post-processing GNSS data (Takasu and Yasuda 2009). All the corrections are import into RTKLIB via graphical user interface (GUI). It can compute PPP in a static or kinematic mode and other several positioning tasks.

In literature, researchers adopt different online PPP services to determine and analyze station coordinates in both static and kinematic mode. SF and/or DF of GPS, as well as combined GPS/GLONASS system, are often used for the PPP performance analysis. Some work about the precision of the positioning results using online Canadian Spatial Reference System CSRS-PPP service has been reported (Choy et al., 2013; Dawidowicz and Krzan, 2014; Farah, 2018; Krasuski, et al., 2018). An analysis of precision and the accuracy of the position determination of GPS-only and combined GPS/GLONASS measurements using online MagicGNSS service has been investigated (Ocalan et al., 2013; Yigit et al., 2014; Anquela et al., 2013). Recently, GPS and GLONASS SF observations from Ethiopian IGS stations are used for kinematic test using Net_Diff software. Calculations showed that three-dimensional root mean square (RMS 3D) is within 0.273 and 0.816 m for GPS PPP and improved from 0.256 to 0.550 m for the combined GPS/GLONASS PPP solutions (Hamed et al., 2019).

However, previous studies analyzed and computed station coordinates using online GNSS data processing services. Studies about evaluation and assessment of position determination using GPS, GLONASS, and combined GPS/GLONASS systems using open-software packages are very limited. The main focus of this study is to analyze and evaluate the accuracy of static PPP coordinates using recently available open software package GAMP for three different GNSS combinations.

2. GNSS OBSERVATION MODEL

The basic observation equations for GNSS pseudorange (P) and carrier phase (Φ) can be expressed as (Pan et al., 2017);

$$P_{f,r}^{j} = \rho_r^j + c\left(\delta t_r^j - \delta T^j\right) + T_r^j + I_f^j + \varepsilon(P_{f,r}^j) \quad (1)$$

$$\phi_{f,r}^{j} = \rho_r^j + c\left(\delta t_r^j - \delta T^j\right) + T_r^j - I_f^j + N_f^j \lambda_f^j + \xi_{pco} + \xi_{se} + \xi_{ot} + \xi_{rel} + \phi_w + \xi\left(\phi_{f,r}^j\right) \quad (2)$$

where scripts *f, r,* and *j* represent the frequency of satellite (f = 1, 2), receiver, and satellite system, respectively; ρ_r^j is the true geometric range between the satellite and the receiver; c is the speed of light in vacuum (m/s); δt_r^j and δT^j are the receiver and satellite clock offset in seconds, respectively; T_r^j is the slant tropospheric delay in meters; I_f^j is the first-order ionospheric delay in meters; N_f^j is the non-integer carrier phase ambiguity term in cycle; λ_f^j is the carrier wavelength of DF in meters; ξ_{pco}, ξ_{se}, ξ_{ot}, ξ_{rel}, and ϕ_w are satellite and receiver antenna phase center offset (PCO), solid earth tide, ocean tide loading, relativistic effect, and carrier phase wind up corrections, respectively; and $\varepsilon(P_{f,r}^j)$ and $\xi\left(\Phi_{f,r}^j\right)$ are un-modeled measurement errors (noise, multipath) in GNSS code and phase observations, respectively. The tropospheric delay on the path can be split into a hydrostatic (dry) part and a non-hydrostatic (wet) part, which is written as

$$T_r^j = (ZWD.m_w(e) + ZIID.m_h(e) + m_g(e)) \quad (3)$$

where e is the elevation of the satellite; m_w, m_h, and m_g are wet, hydrostatic, and gradient (north-south and east-west components) mapping functions, respectively; and *ZHD* and *ZWD* is the zenith hydrostatic delay and the zenith wet delay, respectively. In Eq. (3), ZHD is modeled using empirical Saastamoinen model (Saastamoinen, 1972); m_h and m_w are retrieved with Global Mapping Functions (GMF; Beohem et al 2006). However, ZWD and gradient function $m_g = [m_{e,w}\ m_{n,s}]^T$ are estimated as unknowns along with other parameters in the PPP model.

If GNSS measurements are made with DF, the ionosphere-free (IF) linear combination makes it possible to completely eliminate the first-order ionosphere delay. Therefore, undifferenced IF linear combinations of multi-GNSS pseudo-range and phase observations can be expressed as (Cai et al., 2013; Kouba and Heroux, 2001)

$$P_{IF,r}^{G} = \rho_r^j + c\left(\delta t_r^j\right) + T_r^j + \varepsilon(P_{IF,r}^G) \quad (4)$$

$$\Phi_{IF,r}^{G} = \rho_r^j + c\left(\delta t_r^j\right) + T_r^j + N_{IF}^G \lambda_{IF}^G + \xi\left(\Phi_{IF,r}^G\right) \quad (5)$$

$$P_{IF,r}^{R} = \rho_r^j + c\left(\delta t_r^j\right) + T_r^j + ISB_{R,G} + \varepsilon(P_{IF,r}^R) \quad (6)$$

$$\Phi_{IF,r}^{R} = \rho_r^j + c\left(\delta t_r^j\right) + T_r^j + N_{IF}^R \lambda_{IF}^R + \xi\left(\Phi_{IF,r}^R\right) \quad (7)$$

where superscripts *G* and *R* represent the GPS and GLONASS system, respectively; $ISB_{R,G}$ is the intersystem bias of GPS and GLONASS system. As GLONASS satellites emit the signals on individual frequencies, it will also lead to frequency-dependent biases in the receivers. For the GLONASS satellites with different frequency factors, the receiver code bias is different. Their differences are usually called inter-frequency biases (IFBs). Therefore,

in combined GPS/GLONASS PPP model, $ISB_{R,G}$ parameter is a combination of inter-frequency code biases of GLONASS system. If we assume that there are k satellites in each GPS and GLONASS satellites, an equation to estimate unknown parameters in a state space vector X can be written as (Cai et al., 2015; Pan et al., 2017)

$$X = [\Delta_{x,y,z}, \delta t_r^j, T_{zwd}, ISB_{R,G}, N_{IF}^{G,1}, \dots, N_{IF}^{G,k}, N_{IF}^{R,1}, \dots, N_{IF}^{R,k}] \quad (8)$$

The vector X includes three station coordinate correction terms (x, y, z), receiver clock offset δt_r^j, tropospheric zenith wet delay T_{zwd}, two system time biases $ISB_{R,G}$, and real values ambiguity parameters of each observed satellites. Appropriate stochastic models are required in order to combine and estimate parameters of different GNSS measurements (Geng et al., 2010). International GNSS service Multi-GNSS Experiment IGS-MGEX precise satellite orbit and clock products are used in order to mitigate the orbit and clock errors (Montenbruck et al., 2017). Other effects such as satellite and receiver antenna PCOs and phase center variations (PCVs), differential code biases (DCBs), solid earth tides, phase wind-up, and relativistic effects must be considered in combined GNSS PPP technique (Guo et al., 2017).

3. SOFTWARE INTRODUCTION AND CAPABILITIES

GAMP (GNSS Analysis software for Multi-constellation and multi-frequency Precise positioning) is an open-source software, which is a modification of RTKLIB (Takasu and Yasuda 2009). It focuses on the multi-GNSS (GPS, GLONASS, Galileo, BeiDou, and QZSS (Quasi Zenith Satellite System)) single point (SP) positioning and PPP using undifferenced and uncombined GNSS observations. The source code can be accessed via the GPS Toolbox web-link https://www.ngs.noaa.gov/gps-toolbox/GAMP. The GAMP software is written in the platform-independent ANSI C language. It can compile and run on different operating systems, such as Windows, UNIX/Linux, and Macintosh (Zhao et al., 2018).

To avoid any blunders in PPP solutions, receiver clock drift with GNSS time system receiver clock inconsistencies are repaired and constructed. Cycle slips are detected in two different combinations, that is, Melbourne–Wübbena (MW) combination and the other is geometry-free (GF) combination. The GF observables are influenced by cycle slips, ionospheric variations, and carrier phase multipath effects, whereas the MW observables are affected by cycle slips, pseudorange noise, and multipath effects. GLONASS code IFBs can be handled in four different schemes, that is, (1) neglecting IFBs, (2) modeling IFBs as a linear or quadratic polynomial function of frequency numbers, (3) estimating IFBs for each GLONASS frequency number, and (4) estimating IFBs for each GLONASS satellite. GAMP provides output in a unified text format; the results contain station coordinates (X, Y, Z) and (East, North, Up) in earth-centered earth-fixed (ECEF) and topocentric coordinate system, pseudorange and carrier phase residuals, and slant total electron content (sTEC) etc.

4. PERFORMANCE METHODOLOGY

4.1 Experiment site

Ten-day data set is collected from 10 IGS stations that are distributed around the globe from January 7 to 16, 2018. IGS sites are also designated as MGEX stations, which are equipped with multi-GNSS receivers that can simultaneously track and provide the DF observations from GPS, GLONASS, Galileo, and BeiDou satellites. Geographic location of IGS stations are shown in Figure 1. Table 1 presents the geodetic coordinates (latitude, longitude), receiver type, and antenna of the IGS study sites.

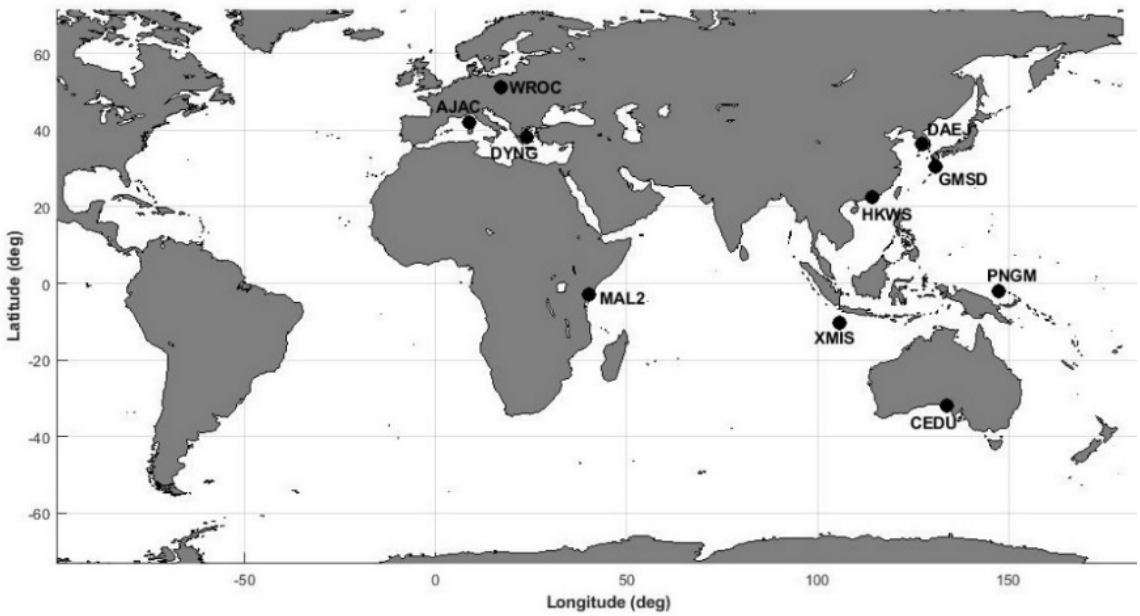

Figure 1. Geographical distribution of IGS stations used in this study

Table 1. Information about coordinates, receiver, and antenna of the IGS MGEX stations.

Site	Location	Coordinates		Receiver	Antenna
		Latitude	Longitude		
WROC	Poland	51.1133	17.0620	LEICA GR50	LEIAR25.R4
HKWS	Hong Kong	22.4343	114.3354	LEICA GR50	LEIAR25.R4
MAL2	Kenya	−02.9960	040.1939	SEPT POLARX4	LEIAR25.R4
AJAC	France	41.9275	008.7626	LEICA GR25	TRM57971.0
CEDU	Australia	−31.8667	133.8098	SEPT POLARX4	AOAD/M_T
DAEJ	S. Korea	36.3994	127.3745	TRIMBLE NETR9	TRM59800.0
DYNG	Greece	38.0786	023.9324	TRIMBLE NETR9	TRM59800.0
GMSD	Japan	30.5564	131.0156	TRIMBLE NETR9	TRM59800.0
PNGM	Popue Guine	−02.0432	147.3660	TRIMBLE NETR9	TRM59800.0
XMIS	Australia	−10.4500	105.6885	TRIMBLE NETR9	JAVRINGANT_DM

Figure 2 shows the mean number of available individual GNSS system and the Position Dilution of Precision (PDOP) of three different GNSS modes (GPS, GLONASS, and combined GPS/GLONASS constellation). PDOP values indicate the quality of satellite arrangements and satellite geometric strength (Pan et al., 2019). Table 2 presents the chart of average visible satellites and the PDOP values shown in the Figure 2.

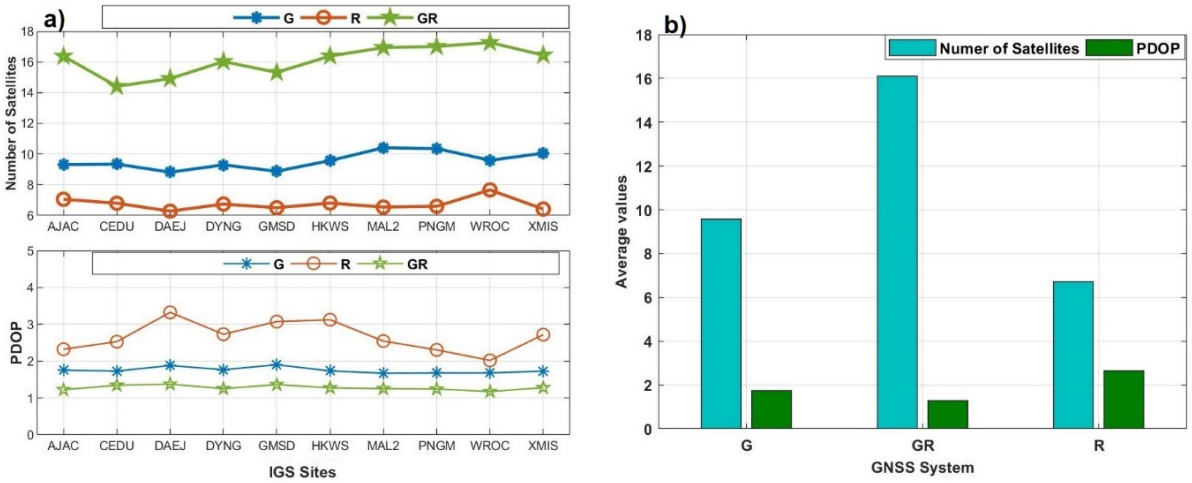

Figure 2. Mean number of available satellites at each IGS sites and average PDOP values represented in (a) and average number of available satellites and corresponding PDOP values of GPS, GLONASS, and combined GPS/GLONASS system represented in (b)

Table 2. Average number of visible satellites and corresponding PDOP values of each IGS sites for GPS, GLONASS, and combined GPS/GLONASS constellation.

Site	GPS		GLONASS		GPS/GLONASS	
	Average Satellites	PDOP	Average Satellites	PDOP	Average Satellites	PDOP
WROC	9.59	1.68	7.66	2.02	17.27	1.17
HKWS	9.57	1.74	6.80	3.12	16.39	1.27
MAL2	10.41	1.67	6.54	2.55	16.93	1.25
AJAC	9.32	1.75	7.05	2.32	16.37	1.23
CEDU	9.34	1.73	6.79	2.53	14.41	1.35
DAEJ	8.82	1.88	6.28	3.33	14.91	1.38
DYNG	9.29	1.77	6.74	2.73	16.02	1.25
GMSD	8.88	1.90	6.50	3.07	15.32	1.36
PNGM	10.36	1.68	6.59	2.31	17.01	1.24
XMIS	10.05	1.73	6.41	2.72	16.45	1.28
∑	9.56	1.75	6.74	2.67	16.11	1.28

It can be demonstrated from Table 2 that, on an average, minimum of 8.82 and maximum of 10.41 GPS satellites are available at DAEJ and MAL2 stations, respectively, and their corresponding PDOP value is 1.88 and 1.67, respectively. However, minimum of 6.28 and maximum of 7.66 GLONASS satellites are available at stations DAEJ and WROC,

respectively, and their corresponding PDOP value is 3.33 and 2.02, respectively. With the addition of GLONASS observations with the GPS measurements further increased the satellite availability at DAEJ, MAL2 and WROC stations to about 14.91, 16.93, and 17.27, respectively, and the PDOP values decreased to 1.38, 1.25, and 1.17, respectively. It can be inferred from Figure 2 that the combined GPS/GLONASS satellites increase the distribution of satellites in the sky and consequently decreased the PDOP values at all IGS stations. From Figure 2, it can be illustrated that the average number of GPS satellites tracked at IGS sites is 9.56 and the corresponding PDOP value is 1.75, which shows an improvement of 33.20% over PDOP value of GLONASS system. On the other hand, combined GPS/GLONASS system increased the number of available satellites and significantly reduced the PDOP value. In addition, the average PDOP value of GPS/GLONASS combined mode is improved by 27.03% and 51.32% over GPS and GLONASS system, respectively.

4.2 PPP performance strategy

All the 24-hour observations are sampled at 30-s interval. Table 3 presents the PPP processing strategy adopted for PPP solution. Station coordinates are considered as time constant. Standard deviation (STD) is considered as a quality indicator for the PPP performance analysis. The initial STD values for the code and phase is 0.3 and 0.003 m for both GPS and GLONASS observations, respectively. For combined GPS/GLONASS PPP, the system weighting ratio of GPS to GLONASS is 1:1. The spectrum densities for ambiguity parameters and zenith tropospheric delay are set to 1.0×10^{-7} m/s$^{0.5}$ and 1.0×10^{-4} m/s$^{0.5}$, respectively.

For the analysis of kinematic/dynamic platform, the ambiguities are treated as constants, and other parameters are all epoch dependent. Therefore, GNSS observations are processed for the current epoch and the next epoch; hence, parameters in Kalman filter (KF) must be estimated for each epoch. Intersystem biases/inter-frequency biases are estimated as arc-dependent constants for each receiver or receiver-satellite link pair. The precise orbit and clock products provided by German Research Centre for Geosciences, GFZ (one of MGEX Analysis Centers), with a sampling rate of 300 s and 30 s, respectively, are adopted for orbit and clock corrections. For the analysis of positioning accuracy, the data set is processed in three different PPP combinations, that is, GPS-only, GLONASS-only, and GPS/GLONASS PPP mode. The precise coordinates of IGS stations are obtained from IGS Solution Independent Exchange format (SINEX) daily files. Table 3 presents the PPP processing strategy adopted in this study for PPP solution. GPS and GLONASS code and carrier phase residuals are computed 24 hours after data processing.

Table 3. PPP performance analysis strategy

GNSS system	GPS, GLONASS
Platform	Static only
Observables	Undifferenced ionosphere-free dual-frequency observations
Satellite orbit and clock	Final precise MGEX products (by GFZ Analysis Center)
Satellite antenna phase center (PCOs/PCVs)	IGS antenna model IGS14.atx
Receiver antenna phase center (PCOs/PCVs)	IGS antenna model IGS14.atx
Differential code biases	Convert C1 to P1 code observations using CODE Analysis Center products
Ionosphere delay	First order removed by IF linear dual-frequency observations
Troposphere Dry component Wet component	 A priori values are used from Saastamoinen model Estimated using the Global Mapping Function: GMF
Estimator	Kalman Filter
Elevation mask	7^{0}
Weighting method	Elevation-dependent weights *1/sin (elevation)*
Priori observation	Carrier phase: 0.003 m and code pseudoranges: 0.3 m at zenith
ISB	Time constant
GLONASS IFBs	Intersystem bias + interchannel bias for every satellite (ISB+ICB)
Solid earth tide, relativistic effect Ocean Tide Loading Phase Wind up	Corrections applied (IERS 2010) Petit and Luzum 2010 Wu et al, 1993
Coordinates	Considered as constant
Output Analysis	Position (East, North, Up), Receiver clock bias, 3D Positioning error, Residuals Tropospheric zenith total delay

5. RESULTS AND DISCUSSION

5.1 Evaluation of GPS, GLONASS, and combined GPSS/GLONASS PPP

Figure 3 shows positioning errors in east, north, and up components; the average satellite number; and PDOP values for GPS-only, GLONASS-only, and combined GPS/GLONASS cases at DAEJ station for the day of the year (DOY) 012 and at HKWS station for the DOY 013. Figure 3 clearly demonstrates that the total satellite number is increased and the PDOP value is significantly reduced by adding the GLONASS observation with the GPS measurements. It can be inferred from Figure 3 that, during 24-hour observations, the average

of 8.86, 6.01, and 14.78 satellites are available for the GPS-only, GLONASS-only, and combined GPS/GLONASS systems at DAEJ station, respectively. Moreover, PDOP values for GPS-only system are improved by 65.62% over GLONASS-only system. On the other hand, the PDOP values of combined GPS/GLONASS showed an improvement of 74.68% and 26.35% over GLONASS-only and GPS-only systems, respectively. Similarly, It can be illustrated from Figure 3 that the total satellite number are significantly increased and PDOP values are decreased with the addition of GLONASS observation with the GPS-alone system at HKWS station.

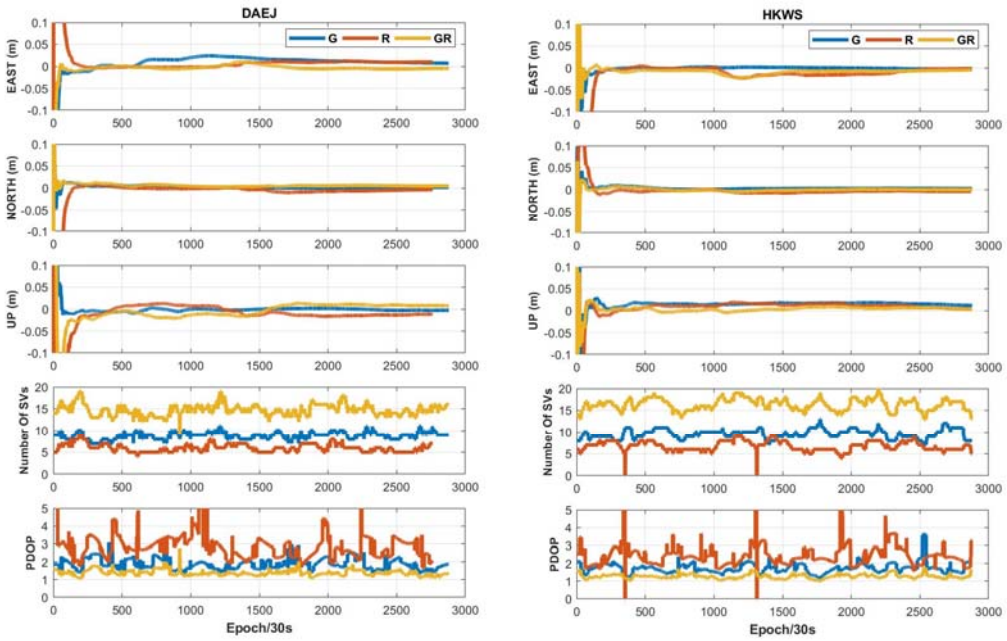

Figure 3. Positioning errors in east, north, and up components; the average satellite number and PDOP values for GPS-only, GLONASS-only, and combined GPS/GLONASS cases at station DAEJ on DOY 012 and at station HKWS on DOY 013

Figure 4 shows the bar diagram of STD of east, north, and up component for GPS-only, GLONASS-only, and combined GPS/GLONASS PPP solutions at DAEJ and HKWS. Table 4 outlines the statistical summary of the positioning errors of GPS-only, GLONASS-only, and combined GPS/GLONASS PPP modes at two IGS stations shown in Figure 4.

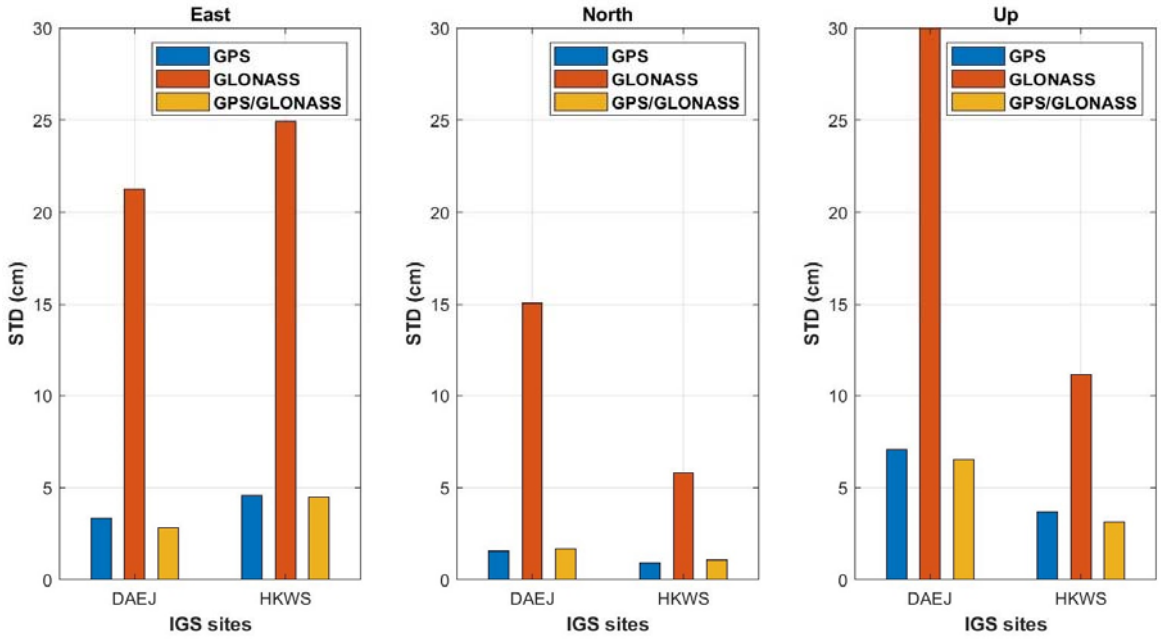

Figure 4. Bar diagram of standard deviation of east, north, and up component for GPS-only, GLONASS-only, and combined GPS/GLONASS PPP solutions at DAEJ and HKWS stations.

Table 4. Statistical summary of positioning errors of the GPS-only, GLONASS-only, and combined GPS/GLONASS PPP modes at DAEJ and HKWS sites (Unit: cm).

Site	Location	GPS		GLONASS		GPS/GLONASS	
		Mean	STD	Mean	STD	Mean	STD
DAEJ	East	0.716	3.359	3.214	21.250	−0.509	2.830
	North	0.245	1.573	−2.450	15.078	0.635	1.670
	Up	0.422	7.057	−4.794	39.343	−0.127	6.528
	3D	2.087	7.743	7.523	47.005	2.180	7.024
HKWS	East	0.023	4.562	−4.171	24.917	−0.666	4.500
	North	0.265	0.916	−0.357	5.803	−0.068	1.083
	Up	1.467	3.695	0.953	11.144	0.373	3.136
	3D	2.105	5.753	5.027	27.783	1.461	5.450

It can be illustrated from Table 4 that GPS-only PPP solutions provides the enhanced positioning accuracy over GLONASS-only mode at DAEJ and HKWS stations. The positioning accuracy of GPS PPP mode is improved by 84.19%, 89.57%, and 82.06% over GLONASS mode in east, north, and up components, respectively. The results from Table 4 also show that combined GPS/GLONASS solutions further increases the positioning accuracy and PPP performance is enhanced with an improvement of 15.75% and 7.50% over GPS-only PPP solution in east and up components at DAEJ site, respectively. However, the positioning accuracy is improved by 1.36% and 15.13% over GPS-only PPP solution in east and up components at HKWS site, respectively. However, it can be seen that combined GPS/GLONASS PPP solution showed insignificant improvement in north component at both the stations. This is attributed that the addition of GLONASS data also increases the number of parameters to be estimated in the space vector, that is, epoch-independent carrier phase

ambiguity and signal multipath for each GLONASS satellite. Moreover, average spatial geometry and number of GPS satellites available are sufficient and good to provide the positioning accuracy at both the stations. Nonetheless, combined GPS/GLONASS PPP solution showed an improvement of 9.29% and 85.06% over GPS-only and GLONASS-only solutions in 3D components, respectively.

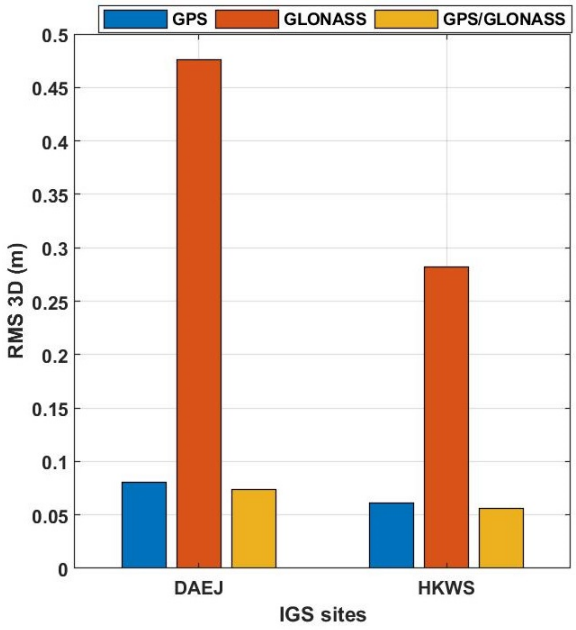

Figure 5. RMS 3D positioning errors of GPS-only, GLONASS-only, and combined GPS/GLONASS systems.

Figure 5 presents RMS 3D of GPS-only, GLONASS-only, and combined GPS/GLONASS solutions at DAEJ and HKWS stations. It can be inferred from Figure 5 that the 3D positioning accuracy is enhanced with the addition of GLONASS observations with GPS-only PPP.

Figure 6 shows the average STD of east, north, and up components; number of satellites; and PDOP values for the three different GNSS combinations of PPP mode. It can be illustrated from Figure 6 that the observation conditions at all IGS sites are obviously different, being located at different geographic locations.

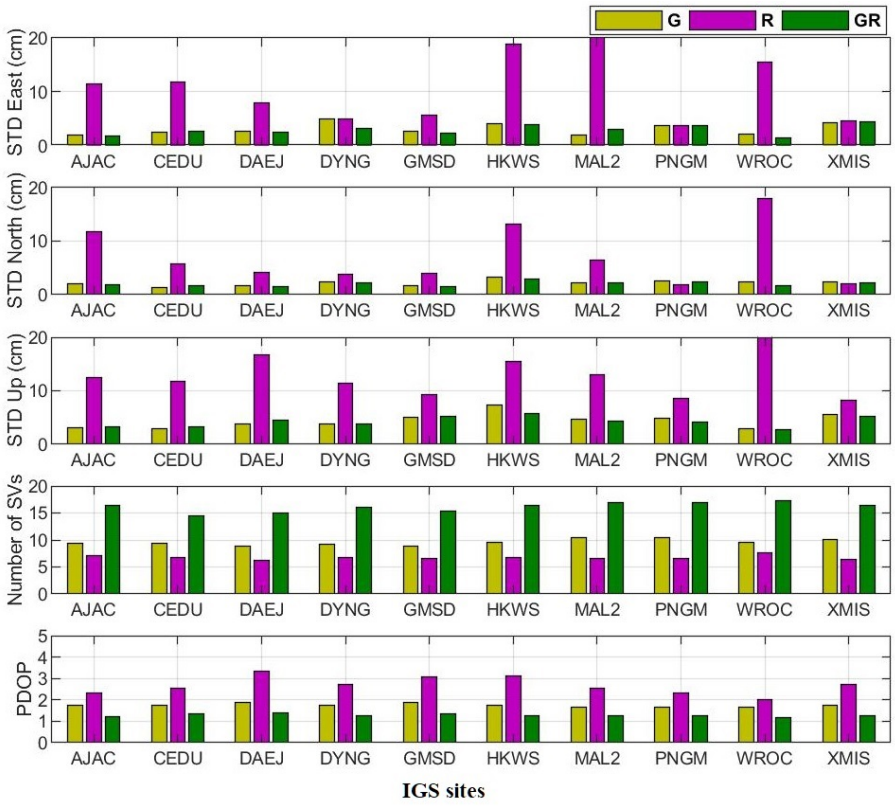

Figure 6. Bar diagram of average STDs of east, north, and up components; number of satellites; and PDOP values for GPS-only, GLONASS-only, and combined GPS/GLONASS PPP solutions.

Figure 7 presents the bar diagram of the STDs of east, north, and up components for the GPS-only, GLONASS-only, and combined GPS/GLONASS PPP modes. Table 5 presents the error statistics of east, north, and up components for GPS-only, GLONASS-only, and combined GPS/GLONASS PPP solutions presented in Figure 7.

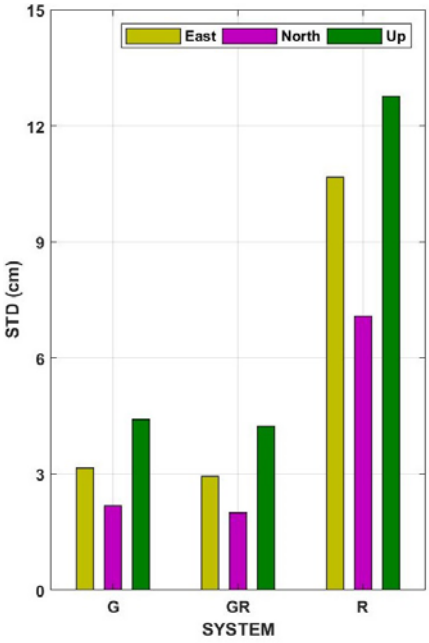

Figure 7. STDs of east, north, and up components for GPS-only, GLONASS-only, and combined GPS/GLONASS systems.

Table 5. PPP error analysis of GPS-only, GLONASS-only, and combined GPS/GLONASS PPP solutions of all IGS stations (Unit: cm).

System	East		North		Up	
	Mean	STD	Mean	STD	Mean	STD
GPS	0.08	3.16	0.10	2.19	0.70	4.42
GLONASS	−0.52	10.66	−0.52	7.08	0.84	12.76
GPS/GLONASS	0.53	2.94	−0.15	2.00	1.00	4.23

It can be illustrated from Figure 7 and Table 5 that the GPS-only solution showed an improvement of 53.74%, 48.71%, and 61.74% over GLONASS PPP solutions in east, north, and up components, respectively. However, adding the GLONASS observations with the GPS-only further increases the PPP solutions. Combined GPS/GLONASS PPP solution is improved by 4.80%, 6.67%, and 2.30% over GPS-only solution and 58.03%, 52.57%, and 63.41% over GLONASS-only solution in east, north, and up components, respectively.

Figure 8 shows the 3D positioning errors of all IGS sites adopted in this study using GPS-only, GLONASS-only, and combined GPS/GLONASS PPP solutions. It can be inferred from Figure 8 that the 3D positioning accuracy is enhanced significantly with the addition of GLONASS observations. On the other hand, GLONASS-only PPP solutions showed worse accuracy as compared with GPS-only solutions.

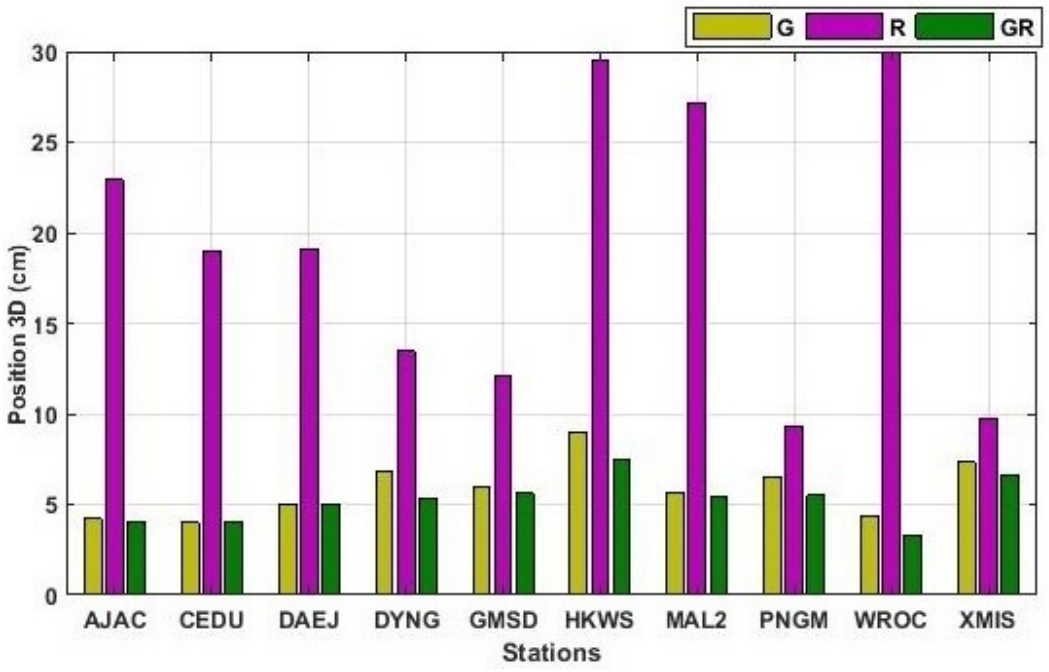

Figure 8. 3D positioning errors using GPS-only, GLONASS-only, and combined GPS/GLONASS PPP systems.

Figure 9 presents the comparison of the 3D positioning of the three different GNSS PPP combination modes. Table 6 presents the error statistics of horizontal and 3D positioning for GPS-only, GLONASS-only, and combined GPS/GLONASS solutions.

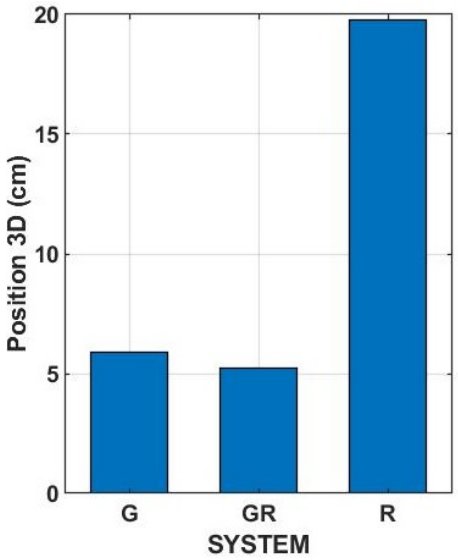

Figure 9. Comparison of 3D positioning of GPS-only, GLONASS-only, and combined GPS/GLONASS systems.

Table 6. PPP positioning errors of GPS-only, GLONASS-only, and combined GPS/GLONASS modes (unit: cm)

System	Positioning Horizontal		Positioning 3D	
	Mean	STD	Mean	STD
GPS	1.20	3.83	2.03	5.89
GLONASS	3.08	13.80	4.49	19.78
GPS/GLONASS	1.97	3.33	3.13	5.23

It can be illustrated that positioning accuracy is significantly enhanced with the combined GPS/GLONASS solutions. The results from the table demonstrate that 3D positioning accuracy of combined GPS/GLONASS PPP system is improved by 10.39% over GPS-only solution and 66.78% over GLONASS only solution.

5.2 Analysis of residuals

In GNSS PPP technique, the observation residuals contain the multipath errors, orbit and clock errors, and measurement noise and other unmodeled errors (Cai et al., 2015). These residuals can be used as an important index for the GNSS observation quality and positioning accuracy.

Figures 10 and 11show the phase and code observation residuals from different satellite systems at MAL2 and WROC on DOY 008, respectively.

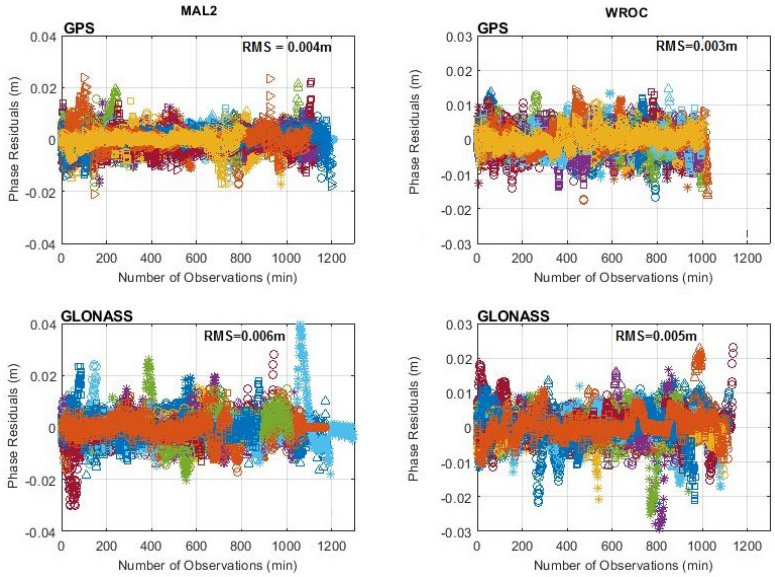

Figure 10. Residuals of phase combination obtained by the GPS and GLONASS PPP solutions at MAL2 and WROC on DOY 008.

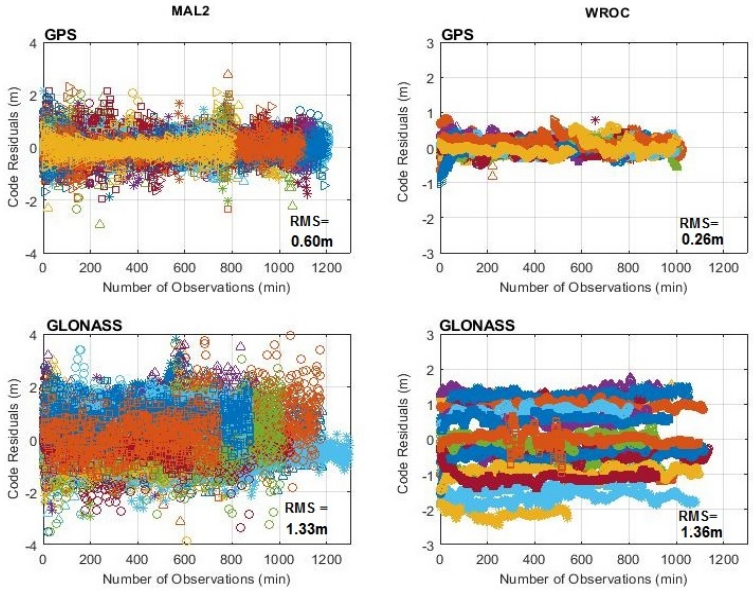

Figure 11. Residuals of code combination obtained by the GPS and GLONASS PPP solutions at MAL2 and WROC on DOY 008.

Different colors represent the different satellites. It can be seen from both the figures that some large discrete code and phase residuals are mainly due to satellites at low-elevation angles. It can be illustrated that the RMS of the phase residuals of GPS and GLONASS is 0.4 and 0.6 cm, respectively. The RMS value of GPS code residuals is within 0.6 m. The RMS value of GLONASS code residuals is within 1.3 m. The value of the code residual results is similar to that from the output analysis in some publications (e.g., Cai and Gao, 2013). GLONASS residuals are much larger compared to GPS. Phase observations are less contaminated by multipath errors, while, phase ambiguity parameters absorbed the constant part, that is, satellite orbit errors.

Figures 12 and 13 depicts the code observation residuals of P1 and P2 for each GPS and GLONASS satellite link observed at MAL2 and WROC stations, respectively. The GPS code observations on each satellite station link is significantly lower than that of the GLONASS satellite. GPS code observation residuals is less than that of GLONASS residuals; this is due to the relatively poor signal quality of GLONASS observations and also the worse contamination of multipath errors for GLONASS code observations. In addition, GPS code observations have negative impact on the multipath errors, and the measurement noise level of GLONASS signals are greater compared with the GPS. It is demonstrated that the GNSS code observation residuals are quite dependent on the satellite elevation (Cai and Gao, 2013)

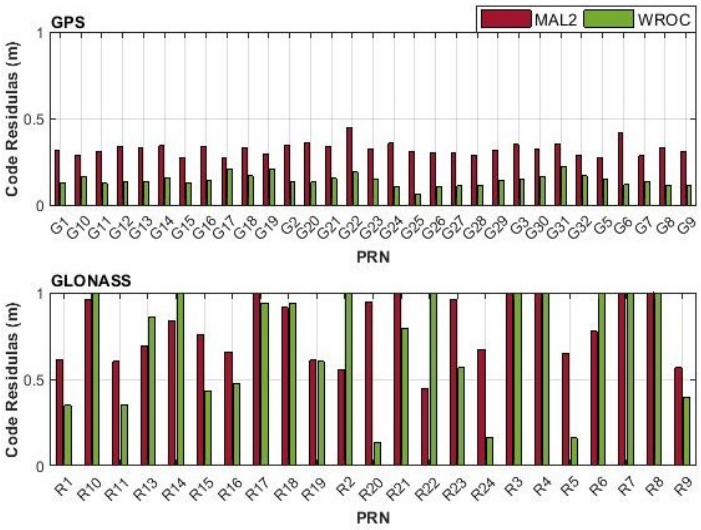

Figure 12. Code observation residuals of P1 of each station-satellite link observed at MAL2 and WROC on DOY 008.

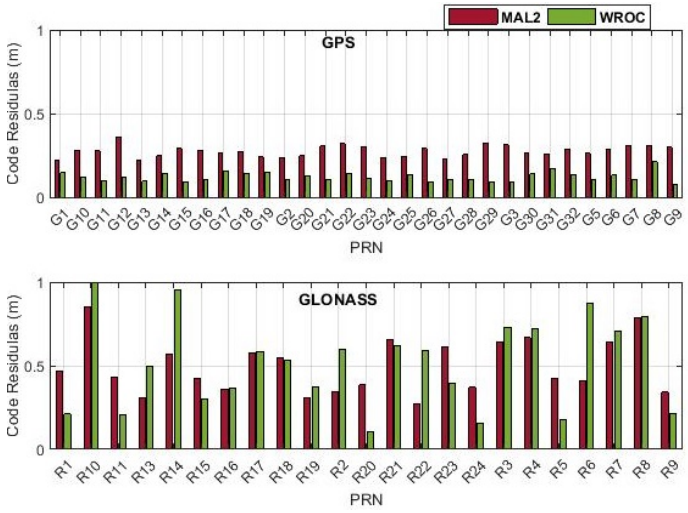

Figure 13. Code observation residuals of P2 of each station-satellite link observed at MAL2 and WROC on DOY 008.

6. SUMMARY AND CONCLUSIONS

The integration of extra satellites from other GNSS system further increased the performance and accuracy of the PPP. This study investigates the capability analysis of recently available multi-GNSS open software package for static PPP method using GPS-only, GLONASS-only, and combined GPS/GLONASS observations. Ten-day data sets from 10 IGS stations are adopted for the positioning solutions. Daily coordinates are estimated using GPS-only, GLONASS-only, and combined GPS/GLONASS PPP modes.

Combined GPS/GLONASS system increased the number of available satellites and significantly reduced the PDOP value. In addition, the average PDOP value for combined GPS/GLONASS mode is improved by 27.03% and 51.32% over GPS and GLONASS systems, respectively. Calculation shows that STD of horizontal component is 3.83, 13.80, and 3.33 cm for GPS-only, GLONASS-only, and combined GPS/GLONASS PPP solutions,

respectively. In addition, STD for 3D component for the GPS-only, GLONASS-only, and combined GPS/GLONASS PPP solutions is 5.89, 19.78, and 5.23 cm, respectively. The calculation results demonstrate that, on an average, combined GPS/GLONASS PPP improves horizontal accuracy by 12.11% and 60.33% and 3D positioning accuracy by 10.39% and 66.78% over GPS-only and GLONASS-only solutions, respectively. In addition, the results also concluded that GPS-only solutions show an improvement of 54.23% and 62.54% over GLONASS-only PPP mode in horizontal and 3D components, respectively. Moreover, residuals of GLONASS IF code observations are larger than the GPS code residuals. However, phase residuals of GPS and GLONASS phase observations are of the same magnitude.

In this study, combined GPS and GLONASS measurements are processed with weighting a ratio of 1. This is because GLONASS IFBs are well modeled and considered, that is, ISB and IFBs for each GLONASS satellites. On the other hand, in view that the precision of the GLONASS code observations are twice lower than the code chipping rate of the GPS code observations, also, if GLONASS IFBs are not taken into account in the processing, then GLONASS code observations should be down weighted to reduce the negative impact of GLONASS IFBs on PPP solutions. Moreover, in this study, satellite elevation angle is set to 7^{o}. GNSS error sources such as the troposphere refraction delay, ionosphere refraction delay, and multipath effect are mostly related to the satellite elevations angles. In addition, signal-to-noise ratio (SNR) and multipath combinations (MPCs) values are strongly correlated with the satellite elevation angles. Previous studies demonstrated that the accuracy of the GPS PPP decreases significantly when the cut-off elevation angle increases. Furthermore, if the observations session length of 30 min is required, the positioning accuracy for the GPS-only PPP is reduced dramatically in horizontal component and is particularly worse in vertical component. However, the accuracy of multi-GNSS (GPS, GLONASS, Galileo, and BeiDou) PPP does not affect with a satellite cut-off angles <40^{o}. Moreover, when the observation session length is >1 hour or even below 30 min, the accuracy of multi-GNSS is not affected by high elevation angles even with <30^{o} to 40^{o} mask angles. Furthermore, the capability of multi-GNSS will significantly increase at very high cut-off elevation in constrained environments, such as in urban canyons or when low-elevation multipath or during the presence of ionospheric scintillations.

Acknowledgement

The author thanks and appreciates the IGS Analysis and Data Center for providing data and GFZ orbit and clock products.

REFERENCES

Anquela, A. Martín, A. Berné, L. Padín, J. (2013). "GPS and GLONASS Static and Kinematic PPP Results." *Journal of Surveying Engineering* 139 (1), 47–58. https://doi.org/10.1061/(ASCE)SU.1943-5428.0000091

Boehm, J. Niell, A. Tregoning, P. Schuh, H. (2006). "Global Mapping Function (GMF): A new empirical mapping function based on numerical weather model data." *Geophysical Research Letter*. 33, 3–6. https://doi.org/10.1029/2005GL025546

Cai, C. Gao, Y. (2013). "Modelling and assessment of combined GPS / GLONASS precise point positioning." *GPS Solution*. 17 (2), 223–236.

Cai, C. Gao, Y. Pan, L. Zhu, J. (2015). "Precise point positioning with quad-constellations: GPS, BeiDou, GLONASS and Galileo." *Advances in Space Research*. 56, 133–143. https://doi.org/10.1016/j.asr.2015.04.001

Choy, S. Zhang, S. Lahaye, F. Héroux, P. (2013). "A comparison between GPS-only and combined GPS+GLONASS Precise Point Positioning." *Journal of Spatial Sciences*. 58 (2),169–190. https://doi.org/10.1080/14498596.2013.808164

Dach, R. Brockmann, E. Schaer, S. Beutler, G. Meindl, M. Prange, L. Bock, H. Jäggi, A. Ostini, L. (2009). "GNSS processing at CODE: Status report." *Journal of Geodesy*. 83, 353–365. https://doi.org/10.1007/s00190-008-0281-2

Dawidowicz, K. Krzan, G. (2014). "Coordinate estimation accuracy of static precise point positioning using on-line PPP service, a case study." *Acta Geodaetica et Geophysica*. 49, 37–55. https://doi.org/10.1007/s40328-013-0038-0

Dong, Z. Jin, S. (2018). "3-D water vapor tomography in Wuhan from GPS, BDS and GLONASS observations." *Remote Sensing*. 10, 1–15. https://doi.org/10.3390/rs10010062

Farah, A. (2018). "Kinematic-PPP using Single/Dual Frequency Observations from (GPS, GLONASS and GPS/GLONASS) Constellations for Hydrography." *Artificial Satellites* 53(1): 37-46.

Geng, J. Meng, X. Dodson, A.H. Teferle, F.N. (2010). "Integer ambiguity resolution in precise point positioning: Method comparison." *Journal of Geodesy*. 84, 569–581. https://doi.org/10.1007/s00190-010-0399-x

GIPSY-OASIS. (2019). Website for GIPSY-OASIS features. Available at: https://gipsy-oasis.jpl.nasa.gov/gipsy/index.php [Accessed July 2019].

Guo, F. Li, X. Zhang, X. Wang, J. (2017). "The contribution of Multi-GNSS Experiment (MGEX) to precise point positioning." *Advances in Space Research*. 59, 2714–2725. https://doi.org/10.1016/j.asr.2016.05.018

Guo, Q. (2015). "Precision comparison and analysis of four online free PPP services in static positioning and tropospheric delay estimation." *GPS Solution*. 19 (4), 537–544. https://doi.org/10.1007/s10291-014-0413-5

Hamed, M. Abdullah, A. Farah, A. (2019). "Kinematic PPP Using Mixed GPS/GLONASS Single-Frequency Observations." *Artificial Satellites* 54(3): 97-112.

Hernandez, M. Juan, J. Sanz, J. Ramos, P. Garcia, A., Salazar, D., Ventura, J. Lopez, C. (2010), The ESA/UPC GNSS-lab tool (gLAB). In Proc. of the 5th ESA Workshop on Satellite Navigation Technologies (NAVITEC' 2010), ESTEC, Noordwijk, The Netherlands

Herring, A. King, W. Floyd, A. McClusky, C. (2015). Introduction to GAMIT/GLOBK, Release 10.6 1–50. Available at: http://www-gpsg.mit.edu/~simon/gtgk/Intro_GG.pdf

Kouba, J. Héroux, P. (2001). "Precise Point Positioning Using IGS Orbit and Clock Products." *GPS Solution*. 5 (2), 12–28. https://doi.org/10.1007/PL00012883

Krasuski, K., Cwiklak, J. Jafernik, H. (2018), "Aircraft positioning using PPP method in GLONASS system", *Aircraft Engineering and Aerospace Technology*, Vol. 90 No. 9, pp. 1413-1420. https://doi.org/10.1108/AEAT-06-2017-0147.

Krasuski, K., Wierzbicki, D. Jafernik, H. (2018), "Utilization PPP method in aircraft positioning in post-processing mode", *Aircraft Engineering and Aerospace Technology*, Vol. 90 No. 1, pp. 202-209. https://doi.org/10.1108/AEAT-05-2016-0078

Lagler, K. Schindelegger, M. Böhm, J. Krásná, H. Nilsson, T. (2013). "GPT2: Empirical slant delay model for radio space geodetic techniques." *Geophysical Research Letter*. 40, 1069–1073. https://doi.org/10.1002/grl.50288

Lou, Y. Zheng, F. Gu, S. Wang, C. Guo, H. Feng, Y. (2016). "Multi-GNSS precise point positioning with raw single-frequency and dual-frequency measurement models." *GPS Solution*. 20 (4), 849–862. https://doi.org/10.1007/s10291-015-0495-8

Montenbruck, O. Steigenberger, P. Prange, L. Deng, Z. Zhao, Q. Perosanz, F. Romero, I. Noll, C. Stürze, A. Weber, G. Schmid, R. MacLeod, K. Schaer, S. (2017). "The Multi-GNSS Experiment (MGEX) of the International GNSS Service (IGS) – Achievements, prospects and challenges." *Advances in Space Research*. 59, 1671–1697. https://doi.org/10.1016/j.asr.2017.01.011

Ocalan, T. Erdogan, B. Tunalioglu, N. (2013). "Analysis of Web-Based Online Services for Gps Relative and Precise Point Positioning." *Bol. Cienc. Geod., sec. Artig. Curitiba.* 19, 191–207.

Pan, L. Zhang, X. Li, X. Li, Xin, Lu, C. Liu, J. Wang, Q. (2019). "Satellite availability and point positioning accuracy evaluation on a global scale for integration of GPS, GLONASS, BeiDou and Galileo." *Advances in Space Research*. 63, 2696–2710. https://doi.org/10.1016/j.asr.2017.07.029

Pan, Z. Chai, H. Kong, Y. (2017). "Integrating multi-GNSS to improve the performance of precise point positioning." *Advances in Space Research*. 60, 2596–2606. https://doi.org/10.1016/j.asr.2017.01.014

Saastamoinen, J. (1972). "Contributions to the theory of atmospheric refraction." *Bull. Géodésique.* 46, 279–298. https://doi.org/10.1007/BF02521844

Salazar, D. Hernandez, M. Juan, J. Sanz, J. (2010). "GNSS data management and processing with the GPSTk." *GPS Solution*. 14 (3), 293–299. https://doi.org/10.1007/s10291-009-0149-9

Wanninger, L. (2012). "Carrier-phase inter-frequency biases of GLONASS receivers." *Journal of Geodesy*. 86, 139–148. https://doi.org/10.1007/s00190-011-0502-y

Yigit, O. Gikas, V. Alcay, S. Ceylan, A. (2014). "Performance evaluation of short to long term GPS, GLONASS and GPS/GLONASS postprocessed PPP." *Survey Review* 46 (336), 155–166. https://doi.org/10.1179/1752270613Y.0000000068

Zhou, F. Dong, D. Li, W. Jiang, X. Wickert, J. Schuh, H. (2018). "GAMP: An open-source software of multi-GNSS precise point positioning using undifferenced and uncombined observations." *GPS Solution*. 22 (2), 1–10. https://doi.org/10.1007/s10291-018-0699-9

Received: *2020-01-27*

Reviewed: *2020-04-28, by M. Szołucha, and 2020-04-28*

Accepted: *2020-04-28*